

Solar cycle and solar wind dependence of the occurrence of large dB/dt events

Stephen E. Milan¹, Suzanne Mary Imber¹, Amy L Fleetham¹, and Jesper W. Gjerloev²

¹University of Leicester

²APL-JHU

November 24, 2022

Abstract

We investigate sharp changes in magnetic field that can produce Geomagnetically Induced Currents (GICs) which damage pipelines and power grids. We use one-minute cadence SuperMAG observations to find the occurrence distribution of magnetic field “spikes”. Recent studies have determined recurrence statistics for extreme events and charted the local time distribution of spikes; however, their relation to solar activity and conditions in the solar wind is poorly understood. We study spike occurrence during solar cycles 23 and 24, roughly 1995 to 2020. We find three local time hotspots in occurrence: the pre-midnight region associated with substorm onsets, the dawn sector associated with omega band activity, and the pre-noon sector associated with the Kelvin-Helmholtz instability occurring at the magnetopause. Magnetic field perturbations are mainly North-South for substorms and KHI, and East-West for omega bands. Substorm spikes occur at all phases of the solar cycle, but maximise in the declining phase. Omega-band and KHI spikes are confined to solar maximum and the declining phase. Substorm spikes occur during moderate solar wind driving, omega band spikes during strong driving, and KHI spikes during quiet conditions but with high solar wind speed. We show that the shapes of these distributions do not depend on the magnitude of the spikes, so it appears that our results can be extrapolated to extreme events.

1 **Solar cycle and solar wind dependence of the**
2 **occurrence of large dB/dt events**

3 **S. E. Milan^{1,2*}, S. M. Imber¹, A. L. Fleetham¹, and J. Gjerloev³**

4 ¹School of Physics and Astronomy, University of Leicester, Leicester, UK.

5 ²Birkeland Centre for Space Sciences, University of Bergen, Norway.

6 ³Johns Hopkins University Applied Physics Laboratory, USA.

7 **Key Points:**

- 8 • Large dB/dt “spikes” in ground magnetometer data occur in three local time hotspots
9 in the pre-midnight, dawn, and pre-noon sectors
10 • These are consistent with spikes produced by substorm onsets, omega bands, and
11 the Kelvin-Helmholtz instability, respectively
12 • Spike occurrence is controlled by solar activity, maximising in the declining phase
13 of the solar cycle, esp. solar cycle 23

*Department of Physics and Astronomy, University of Leicester, Leicester LE1 7RH, UK

Corresponding author: Steve Milan, steve.milan@le.ac.uk

Abstract

We investigate sharp changes in magnetic field that can produce Geomagnetically Induced Currents (GICs) which damage pipelines and power grids. We use one-minute cadence SuperMAG observations to find the occurrence distribution of magnetic field “spikes”. Recent studies have determined recurrence statistics for extreme events and charted the local time distribution of spikes; however, their relation to solar activity and conditions in the solar wind is poorly understood. We study spike occurrence during solar cycles 23 and 24, roughly 1995 to 2020. We find three local time hotspots in occurrence: the pre-midnight region associated with substorm onsets, the dawn sector associated with omega band activity, and the pre-noon sector associated with the Kelvin-Helmholtz instability occurring at the magnetopause. Magnetic field perturbations are mainly North-South for substorms and KHI, and East-West for omega bands. Substorm spikes occur at all phases of the solar cycle, but maximise in the declining phase. Omega-band and KHI spikes are confined to solar maximum and the declining phase. Substorm spikes occur during moderate solar wind driving, omega band spikes during strong driving, and KHI spikes during quiet conditions but with high solar wind speed. We show that the shapes of these distributions do not depend on the magnitude of the spikes, so it appears that our results can be extrapolated to extreme events.

Plain Language Summary

One aspect of hazardous space weather is Geomagnetically Induced Currents (GICs), produced by sudden changes in electrical currents flowing in the upper atmosphere related to auroral activity. These GICs can negatively impact technological infrastructure including power grids and pipelines. At present, the relation of GICs to changes in solar activity and conditions in the solar wind is poorly understood. We use “spikes” in magnetic field measured with a global network of ground magnetometers, SuperMAG, as a proxy for GICs. We find that their occurrence is strongly modulated by solar activity, maximising in the declining phase of the solar cycle. We identify three different sources of spikes, where they are most commonly seen, and determine the solar wind and auroral activity that gives rise to them. This information will help to forecast the occurrence of hazardous spikes in future.

1 Introduction

Sudden changes in electrical currents flowing in the ionosphere can induce large currents in conductors near the ground, which can be hazardous for power grids, pipelines, and other technological infrastructure. In this study we investigate where and when these Geomagnetically Induced Currents (GICs) are seen most often, how solar activity modulates GICs, and the solar wind conditions under which they occur. Although it is usually thought that GICs occur during geomagnetic storms, we find a class of activity that can occur during quiet times.

Rather than measuring the induced currents themselves, we study magnetic field measurements made by the SuperMAG network of magnetometers (Gjerloev, 2012), specifically sudden changes in those measurements, often called “large dB/dt ” events, or Ground Magnetic Disturbances (GMDs); for ease of writing we will refer to them as “spikes”. Under extreme conditions it is thought that dB/dt can be as large as several 1000s nT min^{-1} , but even more modest variations of the order of 200 nT min^{-1} can produce severe GICs (Rodger et al., 2017). Although the sources of these spikes are still under debate, three primary candidates are ionospheric currents associated with substorm onset in the pre-midnight sector, omega bands in the dawn sector, and ultralow frequency (ULF) magnetic oscillations in the pre-noon sector produced by the Kelvin-Helmholtz instability (KHI) operating on the flank magnetopause (e.g., Weigel et al., 2002, 2003;

63 Pulkkinen & Kataoka, 2006; Kataoka & Pulkkinen, 2008; Juusola et al., 2015; Ngwira
64 et al., 2018; Engebretson et al., 2020; Apatenkov et al., 2020).

65 Rogers et al. (2020) recently undertook a study of spikes observed in 1-min cadence
66 SuperMAG data to predict “return levels” for “return periods” between 5 and 500 years.
67 They noted main peaks in occurrence associated with the pre-midnight, substorm region,
68 the cusp, and subsolar region. Schillings et al. (2022) performed a similar study and iden-
69 tified two main hotspots of spikes in the pre-midnight and dawn sectors during selected
70 geomagnetic storms. In this study we also identify spikes in SuperMAG data, but per-
71 form a more longitudinal study over all levels of geomagnetic activity during solar cy-
72 cles 23 and 24, years 1995 to 2020. We identify the solar wind conditions that are favourable
73 for spike generation, and study the solar cycle dependence of the spikes.

74 2 Observations and Discussion

75 We use 1-min cadence measurements from the SuperMAG network. The Super-
76 MAG analysis technique (Gjerloev, 2012) subtracts the background field from each com-
77 ponent, and we refer to the residuals as the N (North-South, positive northwards), E
78 (East-West, positive eastwards), and Z (vertical, positive downwards in the northern hemi-
79 sphere and upwards in the southern hemisphere) perturbations. We then refer to large
80 minute-on-minute changes in these perturbations as ΔN , ΔE , and ΔZ “spikes”. If we
81 refer to a spike in any component, we use ΔB . Our method of analysis is similar to pre-
82 vious dB/dt studies using SuperMAG data (Rogers et al., 2020; Schillings et al., 2022).

83 We first investigate the distribution of “Disturbance Polar” magnetic perturbations
84 produced by ionospheric currents at auroral latitudes, which are often referred to as DP1,
85 DP2, and DPY. These are associated, respectively, with substorms, general convection,
86 and cusp dynamics (Obayashi, 1967; Nishida, 1968; Mansurov, 1969; Svalgaard, 1973;
87 Milan et al., 2017). Figure 1 shows the occurrence of perturbations greater than 300 nT
88 in the N , E , and Z components measured by SuperMAG magnetometers, on a grid of
89 2° in magnetic latitude and 0.5 hours in magnetic local time (MLT). The percentage oc-
90 currence of positive (> 300 nT) and negative (< -300 nT) perturbations are shown
91 in red and blue, respectively, on a logarithmic scale. The percentage represents the frac-
92 tion of time in each grid cell that each perturbation is greater than the threshold; this
93 has been normalised to account for the non-uniform latitudinal distribution of Super-
94 MAG stations. Observations from the northern and southern hemispheres are combined,
95 though in the case of the Z component, the polarity of the southern hemisphere mea-
96 surements is reversed, due to the the Z axis pointing into and out of the Earth in the
97 NH and SH, respectively. The 300 nT threshold has been picked somewhat arbitrarily;
98 the shapes of the distributions do not change markedly for other values of the thresh-
99 old. Observations from three representative years are presented: 2008 being in the depth
100 of a solar minimum, 2016 being a year of moderate solar activity (declining phase of so-
101 lar cycle 24), and 2003, a year noted for high geomagnetic activity due to being in the
102 declining phase of the very active solar cycle 23.

103 The observed distributions are consistent with the known structure of the auroral
104 currents, which in the main comprise the eastward and westward electrojets in the dawn
105 and dusk sectors (producing the DP2 pattern), and the westward substorm electrojet
106 in the pre-midnight sector (the DP1 pattern). The westwards currents result in southward-
107 directed perturbations across the midnight and dawn sectors (between 18 and 09 MLT),
108 while the eastward electrojet produces a much more limited region of northwards-directed
109 perturbations in the dusk sector (14 to 19 MLT). The auroral upper and lower electro-
110 jet indices, AU and AL (Davis & Sugiura, 1966), which monitor northward- and southward-
111 directed perturbations respectively, are controlled by these two MLT regions. The peak
112 rate of occurrence of $N < -300$ nT perturbations is 4%, 7%, and 14% in 2008, 2016,
113 and 2003, respectively. The latitude and MLT extents of the positive and negative per-

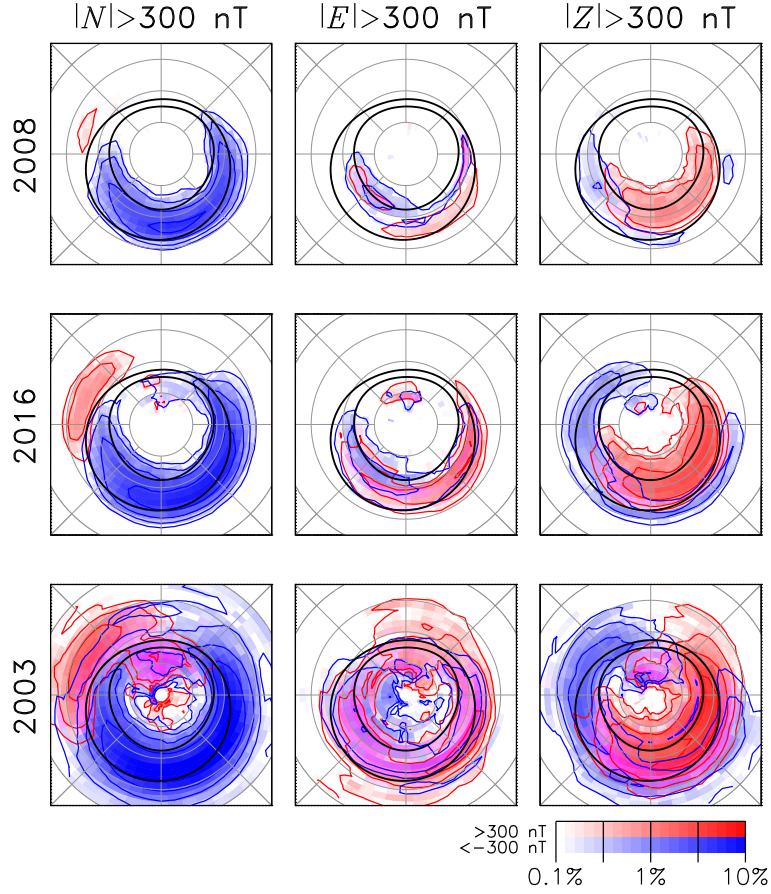


Figure 1. Occurrence distributions of perturbations exceeding ± 300 nT in the N , E , and Z components measured by SuperMAG stations, for three representative years with low, moderate, and high solar activity. Positive and negative perturbations are indicated in red and blue, respectively. The distributions are shown on a magnetic latitude and magnetic local time grid, with noon at the top and dawn to the right; grey circles indicate magnetic latitudes of 80° , 70° , 60° , and 50° . A Feldstein oval for $K_P = 3$ (Feldstein & Starkov, 1967; Holzworth & Meng, 1975) is superimposed for reference.

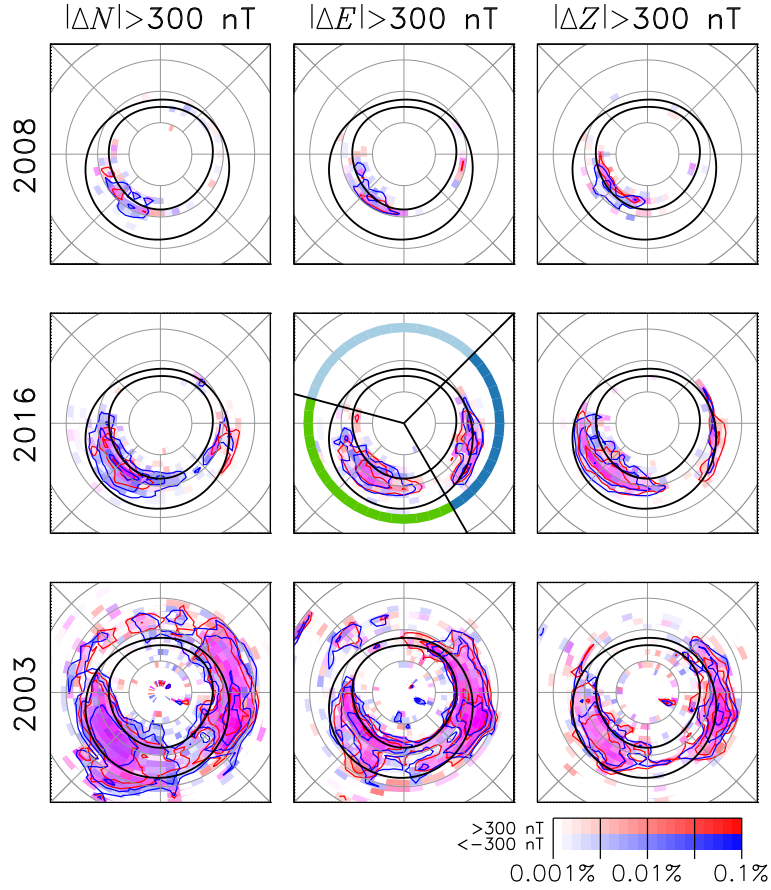


Figure 2. Occurrence distributions of spikes in ΔN , ΔE , and ΔZ exceeding $\pm 300 \text{ nT min}^{-1}$. Presented in a similar format to Figure 1.

114 turbation regions broaden as solar activity increases; in 2003 perturbations were regu-
 115 larly seen at latitudes as low as 50° magnetic latitude. As discussed by Imber et al. (2013),
 116 in 2003 high average solar wind speed combined with high field strength IMF to produce
 117 elevated dayside reconnection rates which resulted in almost double the number of sub-
 118 storms as in each of the previous seven years and pushed the average location of the au-
 119 roral oval to unusually low latitudes.

120 Fewer perturbations were seen in the E and Z components. E perturbations tended
 121 to be positive at dawn and negative at dusk, though very much overlapping in active years.
 122 Z perturbations were negative at dusk; in the dawn sector they were positive at higher
 123 latitudes and negative at lower latitudes, consistent with the expected magnetic signa-
 124 tures of a westward electrojet. Both E and Z perturbations were seen near noon in more
 125 active years, associated with cusp currents producing DPY signatures.

126 We now turn to the occurrence of spikes in the magnetic observations. Figure 2 shows
 127 the occurrence of spikes in the same three years as presented in Figure 1. A spike is de-
 128 fined as two adjacent 1-min data samples in which one or more of the N , E , Z com-
 129 ponents of the magnetic field change by more than 300 nT, that is, $|\Delta N| > 300 \text{ nT}$, $|\Delta E| >$
 130 300 nT , or $|\Delta Z| > 300 \text{ nT}$. Again, the 300 nT threshold is somewhat arbitrary, but we
 131 show below that this does not significantly affect the results. The occurrence distribu-
 132 tions are normalised to the number of magnetometer measurements made in each grid
 133 cell, as in Figure 1.

134 We first consider the results from 2016. In the case of all three magnetic compo-
 135 nents, spikes are observed near auroral latitudes of 64 to 74°, concentrated in two main
 136 local time sectors, which we loosely refer to as pre-midnight (17 to 02 MLT) and dawn
 137 (02 to 09 MLT); these are the same “hotspots” identified by Schillings et al. (2022) and
 138 previous workers. The boundaries of these MLT regions are indicated in the middle panel;
 139 we will refer to the 09 to 17 MLT sector as noon. The pre-midnight hotspot is present
 140 in all three components, but the dawn hotspot is most evident in the E component. In
 141 the N component, the pre-midnight hotspot seems dominated by negative spikes, i.e. $\Delta N <$
 142 -300 nT. In 2008, the number of spikes is reduced, and the dawn hotspot is almost ab-
 143 sent. The pre-midnight spikes are concentrated near high auroral latitudes of 70 to 74°.
 144 Finally, in 2003 many spikes are observed covering latitudes of 54 to 80°. The MLT dis-
 145 tributions are broader, though still concentrated in two hotspots as before.

146 We now investigate the occurrence in spikes for the years 1995 to 2020, which en-
 147 compass solar cycles 23 and 24, shown in Figure 3. Panel (e) shows the monthly (blue)
 148 and smoothed (red) sunspot number. Panel (a) shows the number of spikes of different
 149 magnitudes observed in each year: $|\Delta B|$ greater than 100, 200, 300, and 400 nT min⁻¹;
 150 these are plotted on a logarithmic scale to show that the variation is the same irrespec-
 151 tive of the threshold used. Panel (b) shows the number of spikes, $|\Delta B| > 300$ nT, in
 152 each year on a linear scale, but subdivided by MLT region (17 to 02, 02 to 09, and 09
 153 to 17 MLT, or pre-midnight, dawn, and noon). Panel (c) shows the proportion of spikes
 154 in each MLT region for the same 300 nT threshold. Finally, panel (d) shows the yearly
 155 variation in the number of SuperMAG stations in the northern and southern hemispheres
 156 located above a magnetic latitude of 50°, that is, the number of stations which are able
 157 to observe spikes if they occur. This number varies over the 26 year interval considered,
 158 in general increasing from around 100 in 1995 and plateauing near 190 after 2008.

159 A clear solar cycle dependency in the occurrence of spikes is found. Overall a greater
 160 number of spikes was observed in the more active solar cycle 23 as opposed to 24 (even
 161 though there were more stations operating during cycle 24). Although there are more
 162 spikes at solar maximum than at solar minimum, the number peaks strongly in the declin-
 163 ing phase of each solar cycle, especially in 2003. Very few spikes are seen in the noon
 164 MLT sector, usually less than 10%. Around solar maximum the rest of the spikes are dis-
 165 tributed approximately 50% in the pre-midnight sector and 50% at dawn; at solar min-
 166 imum the split between pre-midnight and dawn spikes is 75% to 25%; during the declin-
 167 ing phase the split is roughly 60% to 40%.

168 We now investigate the MLT dependence of the spikes in more detail, and iden-
 169 tify a third population in addition to the pre-midnight and dawn hotspots. Figure 4 shows
 170 the occurrence distribution of spikes in four representative years, 2019, 2013, 1999, and
 171 2003, roughly in order of increasing solar activity. Each panel shows the MLT distribu-
 172 tion of spikes in each of the components ΔN , ΔE , and ΔZ , normalised to the peak oc-
 173 currence. In 2019, the pre-midnight hotspot dominates, and in this population most spikes
 174 are in the ΔN component. The distribution for 2013 has this same population, but now
 175 the dawn hotspot (04 to 07 MLT) dominates, with ΔE and ΔZ spikes in the majority.
 176 In 1999 the same populations are present, but there is now an increase in ΔN spikes at
 177 dawn, and the dawn hotspot now extends to 08 MLT. The extension of the dawn hotspot
 178 is even more pronounced in 2003, stretching to 10 MLT, and the occurrence of ΔN spikes
 179 has increased again and even dominates in the 07 to 10 MLT sector. We conclude that
 180 there are three populations of spikes: the pre-midnight hotspot, dominated by ΔN spikes,
 181 the dawn hotspot dominated by ΔE and ΔZ spikes, and an additional population of ΔN
 182 spikes in the pre-noon sector. In all years there is a clear dearth of spikes between 10 and
 183 18 MLT, and a similar dearth between 00 and 03 MLT.

184 We will later show that the pre-midnight hotspot is associated with substorm on-
 185 sets, the dawn sector hotspot is consistent with the passage of omega bands, and the pre-
 186 noon hotspot is associated with field-line oscillations. This interpretation is consistent

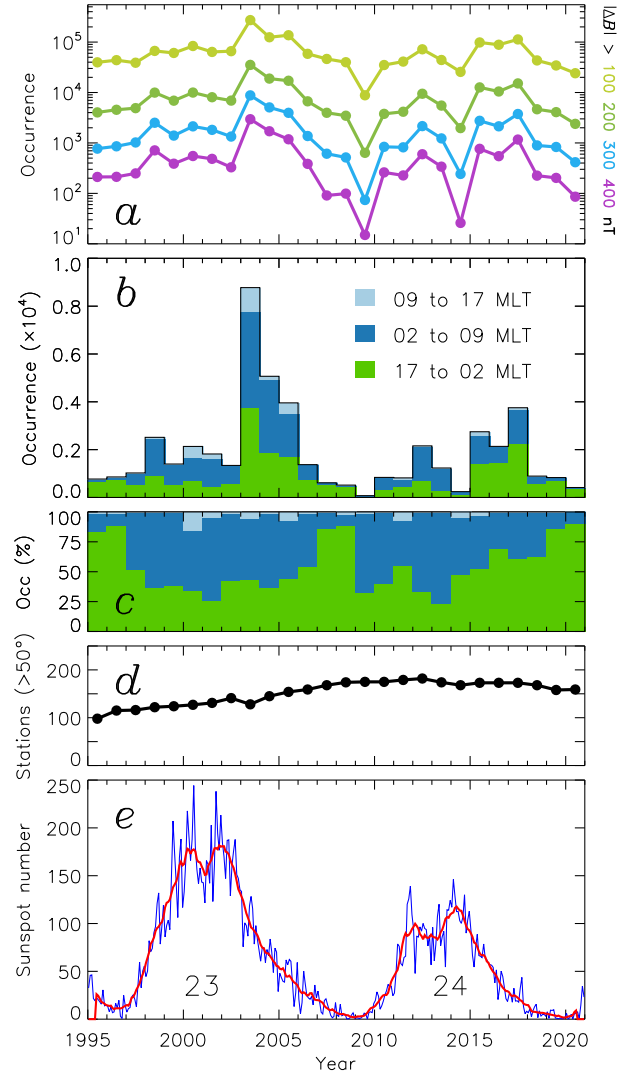


Figure 3. Solar cycle control of the occurrence of spikes. (a) The annual occurrence of spikes with thresholds of $|\Delta B|$ greater than 100, 200, 300, and 400 nT min^{-1} . (b) Annual occurrence of spikes with $|\Delta B| > 300 \text{ nT min}^{-1}$ separated by magnetic local time sector: noon (light blue), dawn (dark blue), and pre-midnight (green). (c) The proportion of spikes seen in each magnetic local time sector. (d) The number of operational SuperMAG stations above 50° geomagnetic latitude (in both hemispheres) in each year. (e). Monthly mean sun spot number (blue) and smoothed (red).

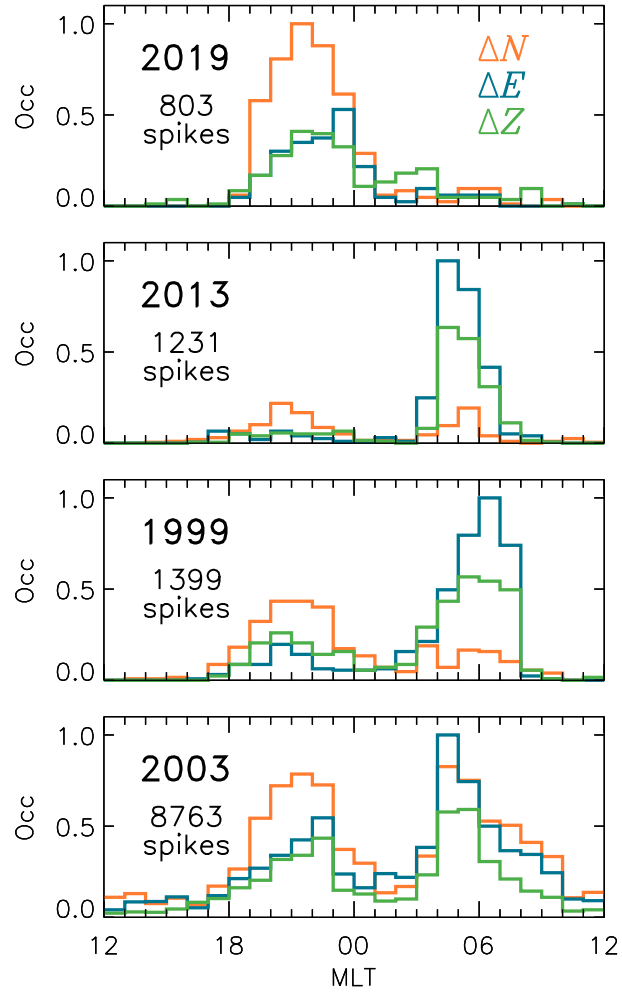


Figure 4. Magnetic local time occurrence distributions of spikes with $|\Delta B|$ greater than 300 nT min^{-1} , in each of the N , E , and Z components, for four representative years from low solar activity (2019) to high solar activity (2003).

187 with previous studies (e.g., Weigel et al., 2002, 2003; Pulkkinen & Kataoka, 2006; Kataoka
 188 & Pulkkinen, 2008; Juusola et al., 2015; Ngwira et al., 2018; Engebretson et al., 2020;
 189 Apatenkov et al., 2020). It is interesting that there is a gap between the pre-midnight
 190 and dawn hotspots, indicating that although omega bands are a substorm recovery phase
 191 phenomenon, they do not propagate from the substorm onset region, but form in the dawn
 192 sector before propagating eastwards. Intense auroral activity can occur in the 00 to 03
 193 MLT sector associated with substorms (Forsyth et al., 2020), but it seemingly does not
 194 give rise to magnetic field spikes.

195 We now turn to a consideration of the solar wind and geomagnetic conditions that
 196 favour the occurrence of spikes in the different MLT sectors. We form occurrence dis-
 197 tributions of spikes as a function of MLT and the simultaneous value of solar wind speed,
 198 V_{SW} , north-south component of the interplanetary magnetic field (IMF), B_Z , a proxy
 199 for the dayside reconnection rate, Φ_D (Milan et al., 2012), the auroral lower electrojet
 200 index, AL, and a measure of the intensity of the ring current, Sym-H, as seen in Figure
 201 5. The solar wind properties and geomagnetic indices are taken from the OMNI dataset
 202 (King & Papitashvili, 2005). The occurrence distributions are formed on a grid with 24
 203 MLT bins along the horizontal axis and 40 bins along the vertical axis. The occurrence
 204 distributions are shown by the contours; grid cells with 10 or more spikes are colour-coded
 205 by the ΔN , ΔE , or ΔZ component that dominates.

206 The pre-midnight, dawn, and pre-noon populations, in which ΔN , ΔE , and ΔZ
 207 spikes dominate, respectively, are apparent in all the occurrence distributions. The pre-
 208 midnight and dawn populations occur over a broad range of V_{SW} , so we conclude that
 209 solar wind speed is not a controlling factor for these spikes. However, the pre-noon pop-
 210 ulation is only observed for high V_{SW} , greater than about 600 km s^{-1} . The pre-midnight
 211 population occurs for relatively modest geomagnetic activity, with the bulk of the dis-
 212 tributions occurring for $-10 < B_Z < 5 \text{ nT}$, $\Phi_D < 100 \text{ kV}$, $\text{AL} > -1000 \text{ nT}$, and
 213 $\text{Sym-H} > -100 \text{ nT}$. On the other hand, the dawn population occurs for more active con-
 214 ditions, $-30 < B_Z < 5 \text{ nT}$, Φ_D up to 300 kV with a peak in the distribution near 175
 215 kV , AL down to -2000 nT , and Sym-H down to -200 nT and below. Finally, the pre-noon
 216 population occurs for quiet geomagnetic activity, with B_Z near 0 nT on average and $\Phi_D <$
 217 50 kV , but as noted before during periods with high solar wind speed, $V_{SW} > 600 \text{ km}$
 218 s^{-1} .

219 We now show three examples of periods with spikes, beginning with Figure 6, en-
 220 compassing 12 hours on 25 January 2003. The bottom three panels show Sym-H, the IMF
 221 B_Y and B_Z components, and the solar wind speed and density. The top four panels con-
 222 centrate on the central 4-hour interval, and show N , E , and Z magnetograms from three
 223 representative SuperMAG stations, and the AU and AL indices. In the SuperMAG pan-
 224 els vertical lines show occurrences of $|\Delta B| > 400 \text{ nT}$ spikes, with the colour indicat-
 225 ing the component containing the spike; several spikes can occur in quick succession, so
 226 some lines appear thicker, but are multiple spikes. The inset in the Sym-H panel is a mag-
 227 netic latitude and magnetic local time dial, showing the locations of SuperMAG stations
 228 when they see spikes during the 4-hour interval (this includes all stations, not just the
 229 three from the top panels). Again, the colour indicates the spike component.

230 In this first example, IMF B_Z is varying back and forth between approximately $+6$
 231 and -6 nT , the solar wind speed is near 700 km s^{-1} and the density is 2 cm^{-3} ; Sym-
 232 H shows that this is a non-storm interval. AU and AL show moderate activity through-
 233 out the period, with an intensification in AL just before 9 UT . The SuperMAG obser-
 234 vations show relatively clear substorm bays in the N component, just before and around
 235 the time of the AL intensification. The stations are located in the pre-midnight sector
 236 at this time, consistent with the interpretation that these spikes are associated with a
 237 relatively intense substorm onset.

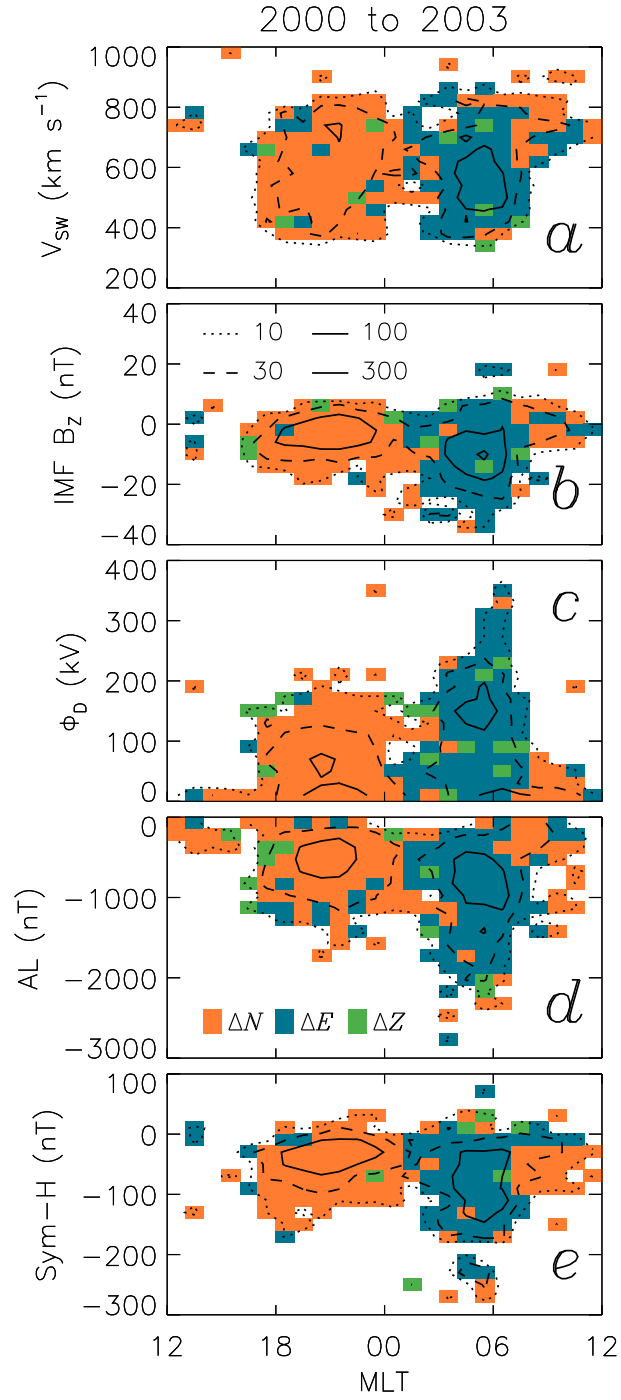


Figure 5. The occurrence rate of spikes as a function of magnetic local time and solar wind and geomagnetic parameters, including (a) solar wind speed, (b) IMF B_z , (c) a proxy for the dayside reconnection rate, Φ_D , (d) the auroral electrojet index AL, (e) the ring current index Sym-H. The occurrence rate is indicated by contours. Where 10 or spikes occur in a single bin, the bin is colour-coded by the dominant component.

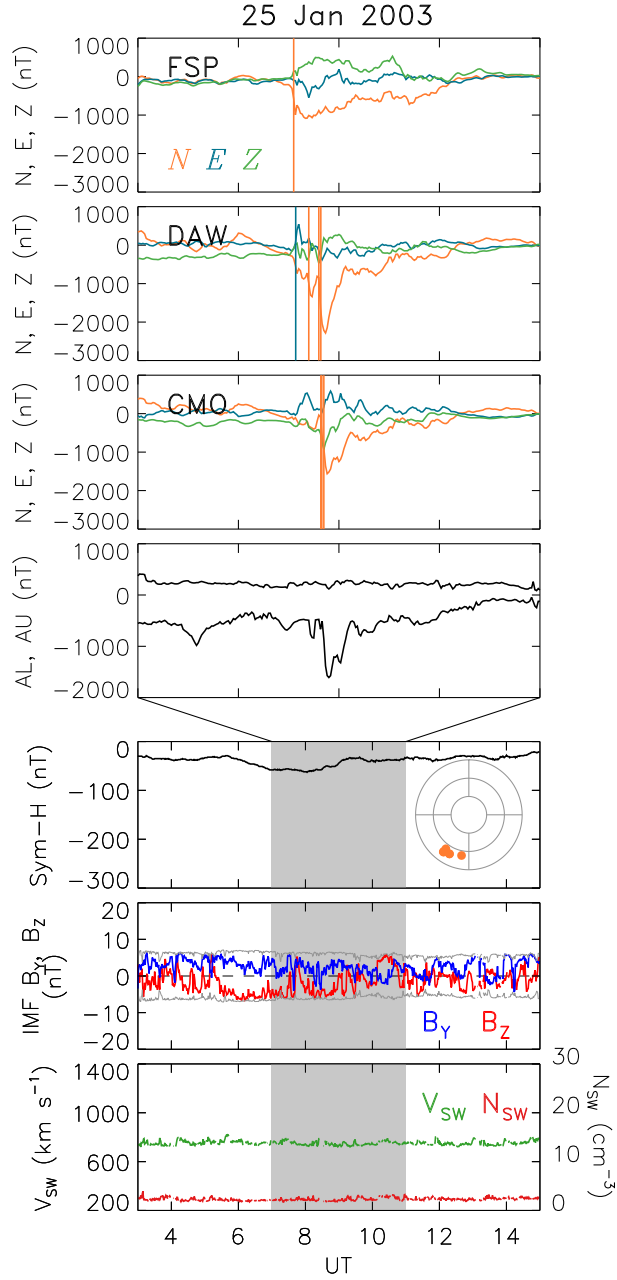


Figure 6. The occurrence of spikes in SuperMAG magnetograms on 25 January 2003. Top three panels, N , E , and Z components of magnetic field for a 4-hour period. Coloured vertical lines indicate the times of greater than 400 nT min^{-1} jumps in a component. The next panel shows the AU and AL electrojet indices. The bottom three panels show the context over a 12-hour period, including the Sym-H index, The B_y and B_z components of the IMF, and solar wind speed and density. The inset panel shows the magnetic latitude and magnetic local time of spikes observed over the 4-hour interval. Concentric circles are in steps of 10° , and noon is at the top. The solar wind and geomagnetic activity indices shown were sourced from OMNIWeb.

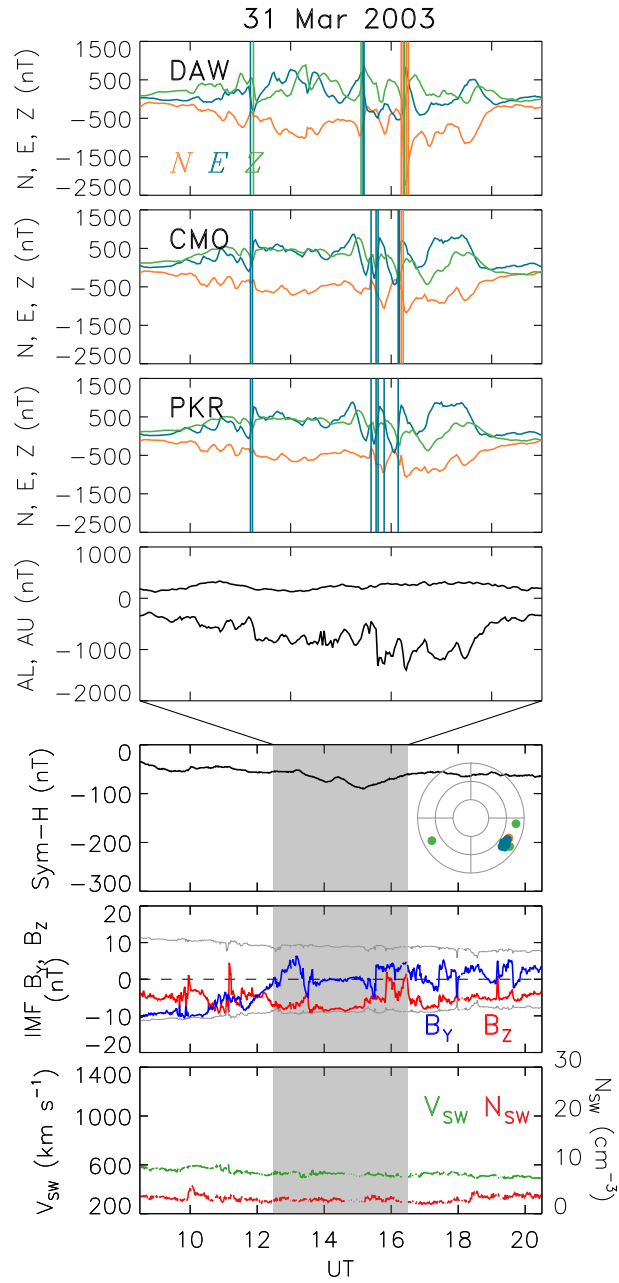


Figure 7. Similar to Figure 6, but for 31 March 2003.

238 The second example shown in Figure 7 is from 31 March 2003. IMF B_Z is near -8
 239 nT throughout most of the interval, and the solar wind speed is near 600 km s^{-1} . AU
 240 and AL show that this is an interval of quite high activity, AL near -1000 nT , but Sym-
 241 H is only -50 nT . The SuperMAG observations show wave-like activity with an ampli-
 242 tude near 500 nT and a period close to 10 to 15 mins in all three components, charac-
 243 teristic of Ps 6 pulsations (Rostoker & Barichello, 1980). Spikes greater than 400 nT min^{-1}
 244 are seen in all three components, but mainly E . The stations are located near 04 MLT
 245 when most of the spike activity occurs, and are consistent with the passage of multiple
 246 omega bands over the stations producing the Ps 6 activity (e.g., Sato et al., 2017; Ap-
 247 atenkov et al., 2020).

248 Finally, the third example is shown in Figure 8, from 31 October 2003. The solar
 249 wind speed is in excess of 1000 km s^{-1} , and this is a period of mainly northwards IMF
 250 with B_Z near $+20 \text{ nT}$. Sym-H shows that this is the recovery phase of a geomagnetic
 251 storm with the peak Sym-H less than -300 nT . AU and AL show moderate activity, but
 252 with two substorm-like onsets. However, it is not these substorms that give rise to spikes
 253 observed by SuperMAG, but rather semi-continuous wave activity seen mainly in the N
 254 and Z components, with periods close to 4 mins. The stations are mostly located in the
 255 08 to 09 MLT sector at this time. We conclude that these are field-line oscillations driven
 256 by Kelvin-Helmholtz activity on the dawn flank of the magnetosphere, as a consequence
 257 of the high solar wind speed. Although the KHI has been invoked before to explain spikes
 258 in the pre-noon sector (e.g., Weigel et al., 2003), it is unclear why a similar population
 259 of spikes is absent in the post-noon sector, as the KHI is thought to operate equally on
 260 both flanks of the magnetosphere.

261 3 Conclusions

262 We have investigated the occurrence of sharp changes in magnetic field, which could
 263 give rise to Ground Induced Currents (GICs) detrimental to technological systems, as
 264 measured by SuperMAG magnetometers for the period 1995 to 2020. North-south mag-
 265 netic perturbations showed that significant eastward and westward electrojets were preva-
 266 lent, especially in years of enhanced solar activity. The eastward electrojet is mainly lo-
 267 cated between 14 and 19 MLT, and the westward electrojet between 18 and 09 MLT. We
 268 then looked for jumps or spikes in the perturbations of the order of several $100s \text{ nT min}^{-1}$
 269 and showed that these occurred in two hotspots, one between 18 and 00 MLT, and the
 270 other between 03 and 09 MLT. These have traditionally been interpreted as spikes caused
 271 by substorm onsets and due to the passage of omega bands, respectively, and our obser-
 272 vations are largely consistent with this. It is curious to note a relative lack of spikes in
 273 the 00 to 03 MLT sector, despite this being a frequent site of auroral activity. We then
 274 showed the presence of a third hotspot near 09 MLT, which was consistent with field line
 275 oscillations driven by Kelvin-Helmholtz instability (KHI) activity on the dawn flank of
 276 the magnetosphere. Spikes associated with substorms and KHI occur mostly in the north-
 277 south component, whereas spikes associated with omega bands are mainly found in the
 278 east-west and up-down components.

279 The occurrence of spikes shows significant variation with solar activity: spikes oc-
 280 cur more at solar maximum than at solar minimum, but are most frequent in the declin-
 281 ing phase of the solar cycle. Spikes that do occur at solar minimum are mainly associ-
 282 ated with substorms, but these also maximise in the declining phase. Omega band and
 283 KHI spikes occur at solar maximum and in the declining phase. The occurrence of sub-
 284 storm and KHI spikes peaked sharply in 2003, a year of high geomagnetic activity driven
 285 by high average solar wind speed. We investigated the occurrence of spikes with greater
 286 than 100, 200, 300, and 400 nT min^{-1} . Naturally, the occurrence of spikes decreased with
 287 increasing magnitude. However, the shape of the solar cycle variation for each thresh-
 288 old was similar, indicating that the observed trends can be extrapolated to more intense
 289 spikes.

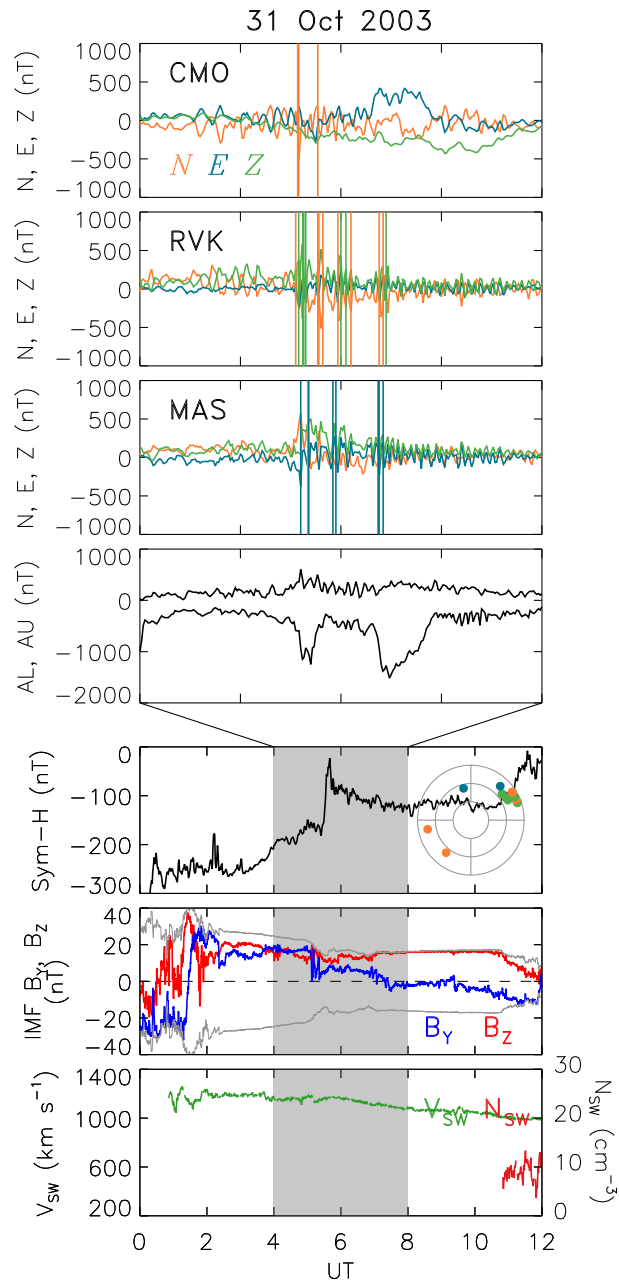


Figure 8. Similar to Figure 6, but for 31 October 2003. The geomagnetic activity indices shown were sourced from OMNIWeb. ACE solar wind data is used due to a data gap in OMNI-Web.

290 Finally, we studied the solar wind conditions and geomagnetic activity levels when
 291 spikes were observed. KHI spikes were observed mainly during fast solar wind, greater
 292 than 600 km s^{-1} , but otherwise generally low geomagnetic activity. Substorm spikes were
 293 observed mostly during more active conditions when the magnetosphere was moderately
 294 driven, IMF $B_Z \approx -5 \text{ nT}$. Omega band spikes occurred under the most active condi-
 295 tions, when the driving was strong, IMF $B_Z \approx -10 \text{ nT}$. Although we have shown an
 296 association between spikes and solar activity and solar wind conditions, it is clearly the
 297 magnetotail plasma sheet that is the ultimate source of the substorm and omega band
 298 phenomena, and further work is required to understand when the plasma sheet responds
 299 in the way that it does.

300 Substorm activity occurs at all phases of the solar cycle, and hence substorm spikes
 301 are observed in all years. However, substorms are more intense when the magnetosphere
 302 accumulates a large amount of open magnetic flux before onset (Milan et al., 2009), and
 303 the polar cap maximises in size during the declining phase of the solar cycle (Imber et
 304 al., 2013). Hence, substorm spikes occur most frequently at such times. Although omega
 305 bands are a substorm-related phenomenon, they are apparently not associated with weak
 306 substorms and hence do not produce spikes at solar minimum. Instead, omega band spikes
 307 are seen at solar maximum and during the declining phase, when solar wind-magnetosphere
 308 coupling is most active. KHI spikes are caused by fast solar wind and so are observed
 309 during the declining phase when solar wind speeds maximise (Imber et al., 2013) due to
 310 the development of low latitude coronal holes on the Sun. Unlike substorms and omega
 311 bands, the KHI does not require ongoing magnetopause reconnection, so southward IMF
 312 is not a necessary condition for the generation of KHI spikes. We note that magnetic field
 313 spikes which can cause GICs are not confined solely to geomagnetic storm conditions.

314 4 Open Research

315 The high resolution (1-min) OMNI data used in this study were obtained from the
 316 NASA Goddard Space Flight Center (GSFC) Space Physics Data Facility OMNIWeb
 317 portal at https://omniweb.gsfc.nasa.gov/form/om_filt_min.html. The 1-min ca-
 318 cadence (“low fidelity”) SuperMAG data were obtained from NASA GSFC through the
 319 SuperMAG portal at <https://supermag.jhuapl.edu/mag/?fidelity=low>.

320 Acknowledgments

321 SEM was supported by the Science and Technology Facilities Council (STFC), UK, grant
 322 nos. ST/S000429/1 and ST/W00089X/1. ALF was supported by an STFC studentship.
 323 The work at the Birkeland Centre for Space Science is supported by the Research Coun-
 324 cil of Norway under contract 223252/F50. We acknowledge use of NASA/GSFC’s Space
 325 Physics Data Facility’s CDAWeb service (at <http://cdaweb.gsfc.nasa.gov>), and OMNI
 326 data.

327 For the SuperMAG ground magnetometer data we gratefully acknowledge: INTER-
 328 MAGNET, Alan Thomson; CARISMA, PI Ian Mann; CANMOS, Geomagnetism Unit
 329 of the Geological Survey of Canada; The S-RAMP Database, PI K. Yumoto and Dr. K.
 330 Shiokawa; The SPIDR database; AARI, PI Oleg Troshichev; The MACCS program, PI
 331 M. Engebretson; GIMA; MEASURE, UCLA IGPP and Florida Institute of Technology;
 332 SAMBA, PI Eftyhia Zesta; 210 Chain, PI K. Yumoto; SAMNET, PI Farideh Honary;
 333 IMAGE, PI Liisa Juusola; Finnish Meteorological Institute, PI Liisa Juusola; Sodankylä
 334 Geophysical Observatory, PI Tero Raita; UiT the Arctic University of Norway, Tromsø
 335 Geophysical Observatory, PI Magnar G. Johnsen; GFZ German Research Centre For Geo-
 336 sciences, PI Jürgen Matzka; Institute of Geophysics, Polish Academy of Sciences, PI Anne
 337 Neska and Jan Reda; Polar Geophysical Institute, PI Alexander Yahnin and Yaroslav Sakharov;
 338 Geological Survey of Sweden, PI Gerhard Schwarz; Swedish Institute of Space Physics,
 339 PI Masatoshi Yamauchi; AUTUMN, PI Martin Connors; DTU Space, Thom Edwards

340 and PI Anna Willer; South Pole and McMurdo Magnetometer, PI's Louis J. Lanzarotti
 341 and Alan T. Weatherwax; ICESTAR; RAPIDMAG; British Antarctic Survey; MacMac,
 342 PI Dr. Peter Chi; BGS, PI Dr. Susan Macmillan; Pushkov Institute of Terrestrial Mag-
 343 netism, Ionosphere and Radio Wave Propagation (IZMIRAN); MFGI, PI B. Heilig; In-
 344 stitute of Geophysics, Polish Academy of Sciences, PI Anne Neska and Jan Reda; Uni-
 345 versity of L'Aquila, PI M. Vellante; BCMT, V. Lesur and A. Chambodut; Data obtained
 346 in cooperation with Geoscience Australia, PI Andrew Lewis; AALPIP, co-PIs Bob Clauer
 347 and Michael Hartinger; MagStar, PI Jennifer Gannon; SuperMAG, PI Jesper W. Gjer-
 348 loev; Data obtained in cooperation with the Australian Bureau of Meteorology, PI Richard
 349 Marshall.

350 References

- 351 Apatenkov, S., Pilipenko, V., Gordeev, E., Viljanen, A., Juusola, L., Belakhovsky,
 352 V., ... Selivanov, V. (2020). Auroral omega bands are a significant cause of
 353 large geomagnetically induced currents. *Geophysical Research Letters*, *47*(6),
 354 e2019GL086677. doi: <https://doi.org/10.1029/2019GL086677>
- 355 Davis, T. N., & Sugiura, M. (1966). Auroral electrojet activity index AE and its
 356 universal time variations. *Journal of Geophysical Research*, *71*(3), 785–801.
- 357 Engebretson, M., Kirkevold, K., Steinmetz, E., Pilipenko, V. A., Moldwin, M., Mc-
 358 Cuen, B., ... others (2020). Interhemispheric comparisons of large nighttime
 359 magnetic perturbation events relevant to GICs. *Journal of Geophysical Re-*
 360 *search: Space Physics*, *125*(8), e2020JA028128. doi: [https://doi.org/10.1029/](https://doi.org/10.1029/2020JA028128)
 361 [2020JA028128](https://doi.org/10.1029/2020JA028128)
- 362 Feldstein, Y. I., & Starkov, G. (1967). Dynamics of auroral belt and polar geomag-
 363 netic disturbances. *Planetary and Space Science*, *15*(2), 209–229.
- 364 Forsyth, C., Sergeev, V., Henderson, M., Nishimura, Y., & Gallardo-Lacourt, B.
 365 (2020). Physical processes of meso-scale, dynamic auroral forms. *Space Science*
 366 *Reviews*, *216*(4), 1–45. doi: <https://doi.org/10.1007/s11214-020-00665-y>
- 367 Gjerloev, J. (2012). The SuperMAG data processing technique. *Journal of Geo-*
 368 *physical Research: Space Physics*, *117*(A9). doi: [https://doi.org/10.1029/](https://doi.org/10.1029/2012JA017683)
 369 [2012JA017683](https://doi.org/10.1029/2012JA017683)
- 370 Holzworth, R., & Meng, C.-I. (1975). Mathematical representation of the auroral
 371 oval. *Geophysical Research Letters*, *2*(9), 377–380. doi: [https://doi.org/10.](https://doi.org/10.1029/GL002i009p00377)
 372 [1029/GL002i009p00377](https://doi.org/10.1029/GL002i009p00377)
- 373 Imber, S., Milan, S., & Lester, M. (2013). Solar cycle variations in polar cap area
 374 measured by the superDARN radars. *Journal of Geophysical Research: Space*
 375 *Physics*, *118*(10), 6188–6196. doi: <https://doi.org/10.1002/jgra.50509>
- 376 Juusola, L., Viljanen, A., Van De Kamp, M., Tanskanen, E., Vanhamäki, H., Par-
 377 tamies, N., & Kauristie, K. (2015). High-latitude ionospheric equivalent
 378 currents during strong space storms: Regional perspective. *Space Weather*,
 379 *13*(1), 49–60. doi: <https://doi.org/10.1002/2014SW001139>
- 380 Kataoka, R., & Pulkkinen, A. (2008). Geomagnetically induced currents during
 381 intense storms driven by coronal mass ejections and corotating interacting
 382 regions. *Journal of Geophysical Research: Space Physics*, *113*(A3). doi:
 383 <https://doi.org/10.1029/2007JA012487>
- 384 King, J., & Papitashvili, N. (2005). Solar wind spatial scales in and comparisons
 385 of hourly Wind and ACE plasma and magnetic field data. *Journal of Geo-*
 386 *physical Research: Space Physics*, *110*(A2). doi: [https://doi.org/10.1029/](https://doi.org/10.1029/2004JA010649)
 387 [2004JA010649](https://doi.org/10.1029/2004JA010649)
- 388 Mansurov, S. (1969). New evidence of a relationship between magnetic fields in
 389 space and on earth. *Geomag. Aeron.*, *9*, 622–623.
- 390 Milan, S., Clausen, L., Coxon, J., Carter, J., Walach, M.-T., Laundal, K., ... others
 391 (2017). Overview of solar wind–magnetosphere–ionosphere–atmosphere cou-
 392 pling and the generation of magnetospheric currents. *Space Science Reviews*,

- 393 206(1-4), 547–573. doi: <https://doi.org/10.1007/s11214-017-0333-0>
- 394 Milan, S., Gosling, J., & Hubert, B. (2012). Relationship between interplanetary pa-
 395 rameters and the magnetopause reconnection rate quantified from observations
 396 of the expanding polar cap. *Journal of Geophysical Research: Space Physics*,
 397 117(A3). doi: <https://doi.org/10.1029/2011JA017082>
- 398 Milan, S., Grocott, A., Forsyth, C., Imber, S., Boakes, P., & Hubert, B. (2009). A
 399 superposed epoch analysis of auroral evolution during substorm growth, on-
 400 set and recovery: Open magnetic flux control of substorm intensity. *Annales*
 401 *Geophysicae*, 27(2), 659–668.
- 402 Ngwira, C. M., Sibeck, D., Silveira, M. V., Georgiou, M., Weygand, J. M.,
 403 Nishimura, Y., & Hampton, D. (2018). A study of intense local dB/dt vari-
 404 ations during two geomagnetic storms. *Space Weather*, 16(6), 676–693. doi:
 405 <https://doi.org/10.1029/2018SW001911>
- 406 Nishida, A. (1968). Geomagnetic DP-2 fluctuations and associated magnetospheric
 407 phenomena. *Journal of Geophysical Research*, 73(5), 1795–1803.
- 408 Obayashi, T. (1967). The interaction of the solar wind with the geomagnetic field
 409 during disturbed conditions. *Solar-Terrestrial Physics*, 107.
- 410 Pulkkinen, A., & Kataoka, R. (2006). S-transform view of geomagnetically in-
 411 duced currents during geomagnetic superstorms. *Geophysical Research Letters*,
 412 33(12). doi: <https://doi.org/10.1029/2006GL025822>
- 413 Rodger, C. J., Mac Manus, D. H., Dalzell, M., Thomson, A. W., Clarke, E., Pe-
 414 tersen, T., ... Divett, T. (2017). Long-term geomagnetically induced
 415 current observations from New Zealand: Peak current estimates for ex-
 416 treme geomagnetic storms. *Space Weather*, 15(11), 1447–1460. doi:
 417 <https://doi.org/10.1002/2017SW001691>
- 418 Rogers, N., Wild, J., Eastoe, E., Gjerloev, J., & Thomson, A. (2020). A global
 419 climatological model of extreme geomagnetic field fluctuations. *Journal of*
 420 *Space Weather and Space Climate*, 10, 5. doi: [https://doi.org/10.1051/swsc/](https://doi.org/10.1051/swsc/2020008)
 421 2020008
- 422 Rostoker, G., & Barichello, J. (1980). Seasonal and diurnal variation of Ps 6 mag-
 423 netic disturbances. *Journal of Geophysical Research: Space Physics*, 85(A1),
 424 161–163. doi: <https://doi.org/10.1029/JA085iA01p00161>
- 425 Sato, N., Yukimatu, A., Tanaka, Y., & Hori, T. (2017). Morphologies of omega band
 426 auroras. *Earth, Planets and Space*, 69(1), 1–11. doi: <https://doi.org/10.1186/s40623-017-0688-1>
- 427 Schillings, A., Palin, L., Opgenoorth, H., Hamrin, M., Rosenqvist, L., Gjerloev, J.,
 428 ... Barnes, R. (2022). Distribution and occurrence frequency of dB/dt spikes
 429 during magnetic storms 1980-2020. *Space Weather*, 20, e2021SW002953. doi:
 430 <https://doi.org/10.1029/2021SW002953>
- 431 Svalgaard, L. (1973). Polar cap magnetic variations and their relationship with
 432 the interplanetary magnetic sector structure. *Journal of Geophysical Research*,
 433 78(13), 2064–2078. doi: <https://doi.org/10.1029/JA078i013p02064>
- 434 Weigel, R., Klimas, A., & Vassiliadis, D. (2003). Solar wind coupling to and pre-
 435 dictability of ground magnetic fields and their time derivatives. *Journal of*
 436 *Geophysical Research: Space Physics*, 108(A7). doi: [https://doi.org/10.1029/](https://doi.org/10.1029/2002JA009627)
 437 2002JA009627
- 438 Weigel, R., Vassiliadis, D., & Klimas, A. (2002). Coupling of the solar wind to
 439 temporal fluctuations in ground magnetic fields. *Geophysical Research Letters*,
 440 29(19), 21–1. doi: <https://doi.org/10.1029/2002GL014740>
- 441